 CMC, vol.20, no.3, pp.205-223, 2010

A Case Study on Mud-Weight Design with Finite-Element Method for Subsalt Wells

X.P. Shen, A. Diaz[1] and T. Sheehy[2]

Abstract: This paper presents a case study for the design of a mud-weight window (MWW) with three-dimensional (3-D), finite-element (FE) tools for subsalt wells. The trajectory of the target well penetrates a 7 km thick salt body. A numerical scheme has been proposed for calculating the shear failure gradient (SFG) and fracture gradient (FG) with 3-D FE software. User subroutines have been developed to address non-uniform pore-pressure distribution.
A series of FE calculations were performed to obtain the MWW of the target wellbore, which consists of the SFG and FG for the subsalt sections. Although no reverse faulting structure exists in the region at the salt base, the stress distribution at some region of the salt base has characteristics of a reverse fault. Additional analyses of the results show that this type of reverse-faulting stress pattern exists only in a small range of depth and width under the salt body. The stress pattern appears to be normal outside of that region. Consequently, a 3-D solution of the MWW along the trajectory has abnormal values at a certain salt base section, which can be 10% greater than the value predicted by 1-D software.

Keywords: Mud-weight window, subsalt wells, finite-element method, shear failure gradient, fracture gradient.

1 Introduction

During the last decade, a significant effort has been made to explore and develop large oil and gas reservoirs associated with salt structures [Dusseault, Maury, Sanfilippo, and Santarelli (2010)]; Jurassic salt emplaced during tertiary (GOM), Late Pennsylvanian to Early Triassic anticlines (Paradox Basin), Mid US continent Devonian Age (Williston Basin), Zechstien-age salt emplaced in the Cretaceous (The North Sea), Zagros salt plugs (Iran), Brazilian and West Africa offshore basins, Kashagan and Tengis Basins in Kazakhstan, etc., are examples of the most active

[1] Halliburton, Houston, TX, U.S.A.
[2] Verdande Technology Inc., TX, U.S.A.

areas of subsalt drilling, which range between 3 km to 7 km of salt body with a total depth below 8.3 km and different salt structural geometries (domes, ridges, salt tongues, pillows, undeformed bedded sedimentary salts, and mixed domains). As a result of the economical success of subsalt reservoir, a significant amount of exploration and new field developments will continue over the next decade in salt provinces, leading to challenges in both designing and drilling wells in these complex geological environments [Tsai, O'Rouke, and Silva (1987)].

Drilling in salt provinces [Whitson and McFadyen (2001)] give rise to two fundamental issues that requires careful management of mud weight: creep rate of salt when drilling into the salt body and pore pressure and fracture gradient determination in both non-salt formations interbedded into the salt and when exiting the salt.

The geometry of a salt body impacts the drilling strategy; in some cases it can limit the well trajectory (salt tongues and bedded salts), and in other cases, it can expand the well trajectory possibilities (diapiric salt) to avoid salt or drilling as much salt as possible according to the geomechanical state of the rock surrounding the salt, depth, and creep rate of the salt.

Owing to the fact that salt is tectonically mobilized by the density difference between salt (2.16×10^3 kg/m^3) and the other sediments (2.3–2.6 $\times10^3$kg/m^3), because of its viscous behavior at moderate load and temperature, the stress field in the surrounding formations is perturbed, leading to stress rotation near the salt-clastic interface and change in stress magnitude that can differ significantly from the far field stresses. As a result, subsalt overpressure or pressure reversion may exist and create extensive rubble or highly-sheared zones below or adjacent to the salt diapirs. This is an intrinsic consequence of the equilibrium stress field needed to satisfy the different stresses that exist within the salt body and the adjacent formation, which causes extremely expensive and difficult wellbore stability problems during drilling, completion, or production, and represents a challenge for the oil industry in both operation and modeling.

Salt affects the actual geomechanical environment through alteration of the local stresses because it cannot sustain deviatoric stress and thus deforms via plastic creep in response to any imposed deviatoric stress, so changes in the stress field and shear stresses adjacent to the salt maybe sufficient to cause reorientation of the principal stress.

As previously mentioned, fundamental wellbore stability problems during drilling in salt environments can be comprised in two critical sections: while drilling through the salt and when exiting the salt.

Wellbore stability problems while drilling through salt are easier to control by han-

dling the density and temperature of drilling fluid. This control is possible because salt behaves like a highly-viscous fluid with a creep rate that is strongly dependent of temperature and stress difference. Salt is impermeable and geochemically inert except in high solubility (easily handled with a saturated water phase in the mud). In addition, salt has a tensile strength (unfractured) that is more reliable than porous formations. Because no pore pressure is present, we can increase the wellbore pressure close to the litho-static pressure inside of the salt without any problem. However, caution should be observed because of the presence of shale intrusion or interbedded bischofite and carnallite. At this stage, increasing mud density, maximizing ROP, over saturating the water phase of the fluid, and cooling the mud are the most common strategies [Whitson and McFadyen (2001)] to control closure rate and washout of the well.

Exiting the salt is the most critical stage in drilling because one can get either a pressure and stress reversion zone leading to a sudden lost-circulation problem or trapped overpressure zones leading to a blowout. As a result, the problem is difficult to anticipate because pore pressure and fracture gradient prediction based on velocity and wireline logging data are impaired by the presence of salt.

The high uncertainty in pore-pressure prediction and the presence of rubble and highly-sheared zones impose the necessity to accurately predict subsalt formation velocities using the most up-to-date techniques in seismic imaging along with numerical simulation to anticipate the appropriate MWW and minimize sub-salt losses [Power, Ivan and Brooks (2003)].

Fredrich, Coblentz, Fossum, and Thorne (2003) reported the results of a 3-D FEM simulation of different geometries of salt bodies: spherical salt bodies, horizontal salt sheets, columnar salt diapers, and columnar salt diapers with an overlaying tongue. Their results show: a) that the shear stress is highly amplified in certain zones in specific geometries adjacent to the salt; b) it induces anisotropy of horizontal stresses, c) the principal stresses are no longer vertical and horizontal, and the vertical stress may not be the maximum stress, d) for some geometries, vertical stress within, and adjacent to, the salt is not equal to the gravitational load (stress-arching effect occurs) before drilling or production and behave similar to the overburden changes during depletion of compactable reservoirs. Finally, they conclude that the only way to determine the stress perturbation is to solve the complete set of equilibrium, compatibility, and constitutive equations with the appropriate initial and boundary conditions using an FEM methodology.

Cullen, Taylor, Thomas, Whitehead, Brudy, and van der Zee (2010) emphasized the importance of 3-D FEM modeling of a subsalt region and discussed the impact of recent technological advances in seismic imaging, pore pressure prediction, and geomechanical modeling to improve drilling efficiency when exiting the salt.

Because of the large differences between field scale and casing-section scale in modeling, it has been difficult, if not impossible, to combine these models in the past. In fact, existing examples of numerical analysis on casing failure were either performed at reservoir scale without direct coupling to behaviors at the field scale or performed at a much larger scale, which sacrificed much needed modeling resolution.

Submodeling techniques are used to accommodate the field-to-casing-section scale discrepancy. The concept of the submodeling technique includes using a large-scale global model to produce boundary conditions for a smaller-scale submodel. In this way, the hierarchical levels of the submodel are not limited. Using this approach, a highly inclusive field-scale analysis can be linked to very detailed casing stress analysis at a much smaller scale. The benefits are bidirectional, with both the larger and smaller scale simulations benefiting from the linkage.

The contents presented in the following sections include: 1) Global model description and numerical results; 2) Model description on submodels and numerical results obtained with submodels; 3) Results obtained with 1-D solution tool; 4) Comparison between results of mud weight window obtained the 3-D FEM and those obtained with 1-D method; 5) Analysis of effective stress ratio in terms numerical results of 3-D FEM; 6) Conclusions.

2 Global Model Description and Numerical Results

2.1 Model description

The field scale model shown in Fig. 1 is a cubic block with a height of 9 km, a width of 8,000 m, and a length of 8,000 m. The salt body is shown in red in Fig. 2. The formation thickness below the salt to the base of the model is in the range of 2,200 to 2,850 m. For the purpose of simplicity without losing accuracy, details of formations below the TVD interval of the reservoir are neglected. Salt geometry is a key factor, which controls stress patterns in its neighborhood. The salt body is represented in Fig. 3. Its thickness along wellbore trajectory is 5,300 m, its width is 6 km, and its axis is in the direction of N30°W, as shown in Fig.4.

As shown in Fig. 5, the model consists of four kinds of materials: 1) top layer, 2) surrounding rock, 3) salt, and 4) base formation. The reservoir is a part of the base formation. Values of material parameters are listed in Table 1.

Loads and BCs of the model are shown in Fig. 1 with normal displacement constraints applied on lateral surfaces and bottom surfaces. Gravity load balanced with initial geo-stress field is applied to every element of the model.

Table 1: Values of material parameters.

Materials	Density kg/m^3	Young's Modulus Pa	Poisson's Ratio	CS/Pa	Friction Angle
Top layer	1,900	1×10^{10}	0.3	elastic	
Salt	2,250	1.3×10^{10}	0.22	4×10^6	25°
Surrounding Rock	2,350	Depth dependent	Depth dependent	1×10^6	25°
Base formation	2,350	Depth dependent	Depth dependent	4×10^6	25°

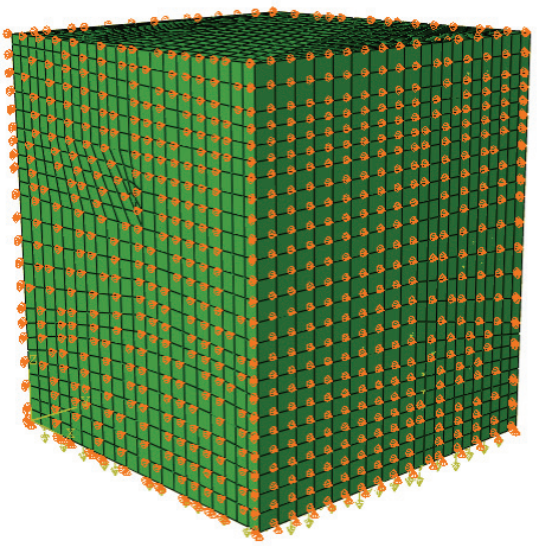

Figure 1: Illustration of global model at field scale: geometry and boundary conditions.

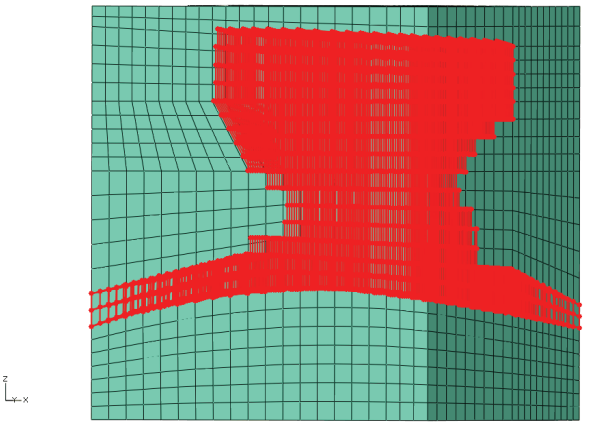

Figure 2: Relative position of salt body to the formations in the model.

2.2 Numerical results of the global model

In Figs. 6 through 8, numerical results obtained with the global model are shown. Fig. 6 shows the distribution of stress σ_x. Fig. 7 and 8 give out the distribution of stress σ_y and σ_z. The section is chosen at the place where wellbore trajectory

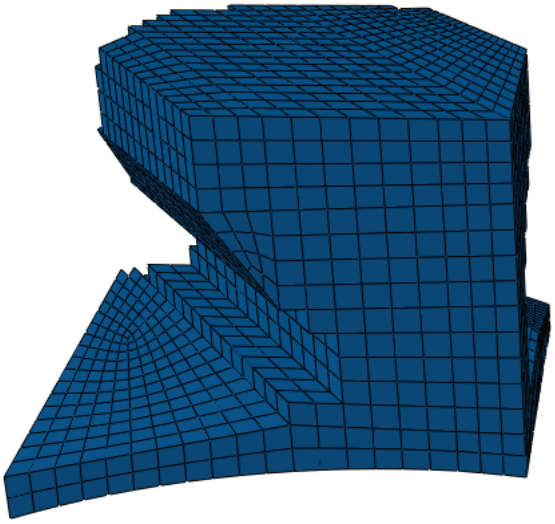

Figure 3: Geometry of the salt body in the model.

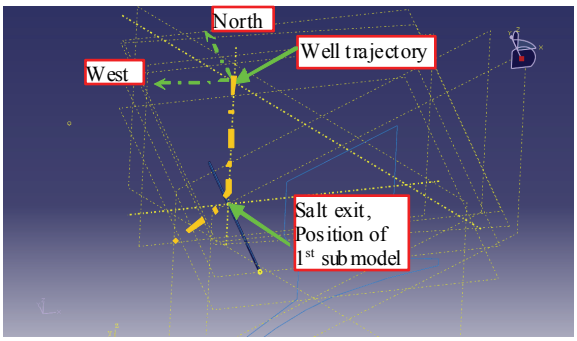

Figure 4: Illustration of wellbore trajectory and the direction of salt's central axis along with salt exit of wellbore.

goes through. The stress shown here is effective stress in which the amount of pore pressure is not included. Sign convention of solid mechanics is followed, which is positive for tensile stress and negative for compression.

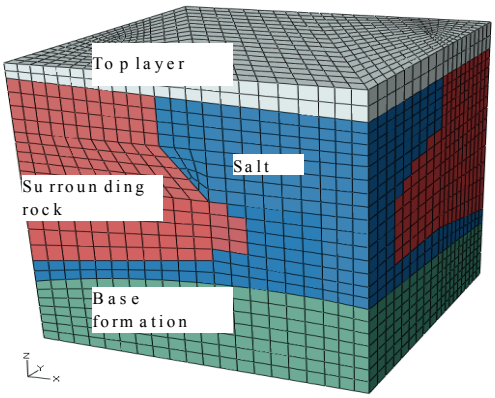

Figure 5: Illustration of various materials used in the model.

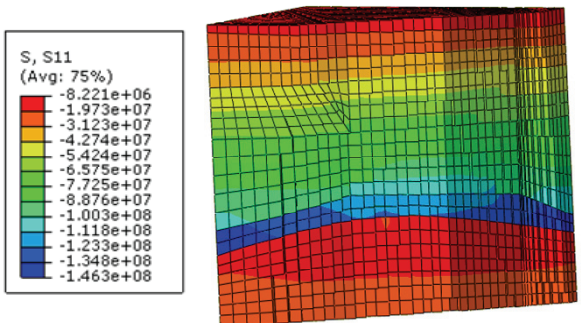

Figure 6: Distribution of stress σ_x in Pa, sectional view.

3 Submodel Description and Numerical Results

3.1 Model description

To overcome the scale discrepancy between the field scale and wellbore section scale, two kinds of submodels have been adopted. The size of the primary submodel has a width and length of 100 m and thickness is 110 m. The size of the secondary submodel has a width and length of 15 m and a thickness of 10 m. Because the wellbore trajectory changes its incline angle with depth, the secondary submodel has 6 sets of values of geometrical parameters to simulate the real wellbore trajectory at each depth interval simulated. For brevity purposes, the details of submodel description are provided for only one set of submodel used here.

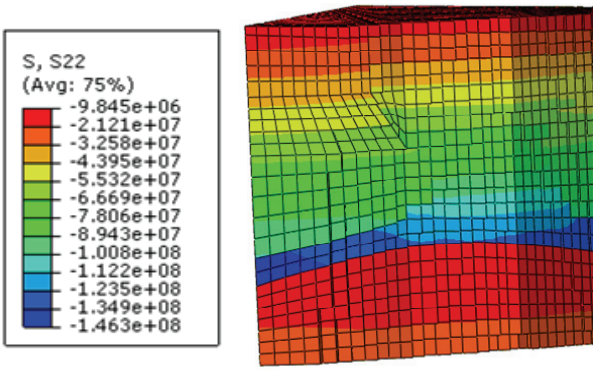

Figure 7: Distribution of stress σ_y in Pa, sectional view.

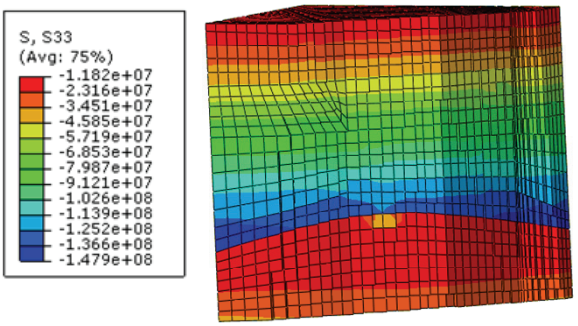

Figure 8: Distribution of stress σ_z in Pa, sectional view.

The function of the primary submodel is only to transfer initial geostress field and displacement boundary conditions from those obtained with the global model to the secondary submodel. Thus, it is not necessary to have wellbore included in it.

The function of the secondary submodel is more important than that of the primary submodel, as it is used to calculate both the SFG and FG of the given wellbore.

In the calculation of SFG for the given wellbore, the drilling process has been simulated in the calculation so as to find the stress variation caused by the drilling process. Thus, it is essential to have the real wellbore geometry (both size and shape and direction) included in the model.

FG required in the mud-weight window is actually selected as the minimum horizontal stress of the initial geostress field. For an inclined wellbore, it is the 'minimum amount of compressive stress' in the petroleum industry. Consequently, the

calculation of FG requires that the wellbore not be drilled.

In this work, the drilling of wellbore will be simulated for the calculation of SFG but will not be simulated in the calculation of FG.

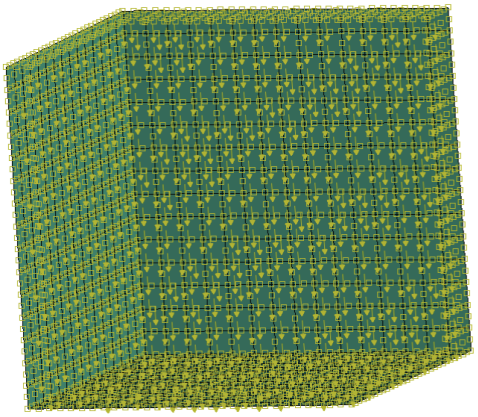

Figure 9: Illustration of the primary submodel.

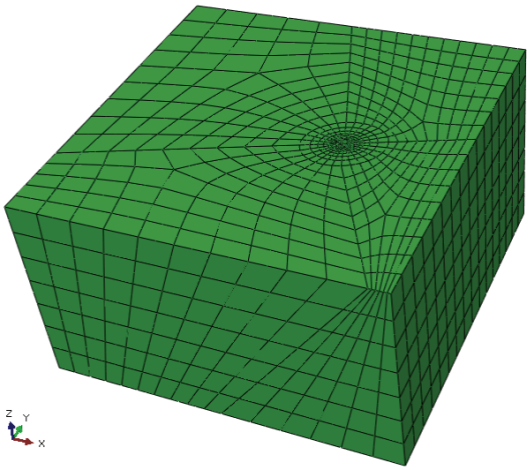

Figure 10: Illustration of the secondary submodel.

3.2 Numerical results of SFG and FG obtained with the secondary submodel

In this subsection, the convention of petroleum industry is adopted for the units of variables, with 1ft=0.3048m, and 1ppg=1174.3Pa/m. As shown in Fig. 11, the green line with blue dot marks represents the pore pressure distribution in the reservoir formation. A TVD depth 19,000 ft is the location in which the wellbore trajectory exits the salt body. The calculation on the mud-weight window focuses on the interval sections below the salt exit. Neglecting the details of the intermediate process, numerical results for SFG and FG obtained with the aforementioned submodel along the given wellbore trajectory are shown in Fig. 11. The thick, red curve with red dots is the SFG, which represents the lower bound of the mud-weight window, and the thinner red curve with square mark is the FG, which represents the upper bound of mud-weight window.

The results of SFG and FG obtained with 1-D software are shown in Fig. 11 for comparison purposes. The dashed, dark blue curve is the SFG solution obtained using the 1-D method, and the solid blue curve is the FG solution obtained with the 1-D method.

A comparison between the 1-D solutions with its corresponding 3-D solutions of SFG and FG shows that a significant difference exists between the two in the TVD interval from 19,000 ft to 21,000 ft. The two sets of results of mud-weight window become almost the same beyond the aforementioned TVD depth. The maximum difference between the two sets of SFG is approximately 1.2 ppg, which occurs at the TVD depth just below 20,000 ft. Accounting for the value of depth, the difference of pressure of mud weight obtained by the 3-D and 1-D methods are significant, and it is necessary to explain why it occurs and which is more reasonable than the other. The analysis is given in the following section.

4 Stress pattern analysis for subsalt formation

The goal of this section is to perform an analysis on the stress pattern in terms of the numerical results obtained with the global model by using FEM. As a measure of stress pattern, the effective stress ratio between three normal stress components of a stress tensor will be visualized and analyzed for the subsalt section of a wellbore. Focus has been put on the stress pattern in the region where the wellbore trajectory goes through. As shown in Fig. 12, the red, vertical line is chosen as Path-1 along which stress distribution will be plotted.

For the convenience of analysis, which is engaged in the framework of solid mechanics, the sign convention and unit convention of solid mechanics will be adopted in the following contexts: negative sign for compression and stress is shown in the unit of Pa.

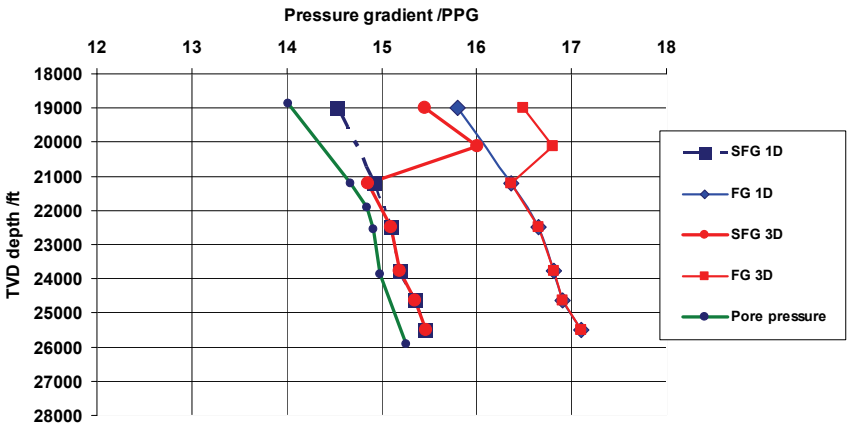

Figure 11: Numerical results of SFG and FG obtained with the secondary sub-model.

Variations of total stress components with z-depth from the top surface along with pore pressure distribution are shown in Fig. 13. The place where non-zero pore pressure occurs is the top of the reservoir formation as well as the salt exit of well-bore trajectory. Effective stress component, σ_z, is given here solely for the purpose of comparison. A close-up view of Fig. 13, which focuses on a 2-km depth interval around the salt-formation interface is given in Fig. 14. As illustrated in Fig. 14, the vertical stress component, σ_z, is the minimum stress component in this depth interval.

The distribution of effective stress ratios along Path-1 is shown in Fig. 16. A close-up view around the salt-reservoir interface for the curves in Fig. 16 is shown in Fig.17. For points in the salt base along Path-1, effective stress ratios are significantly greater than 1. It should be noted that this result is only true for the given Path-1. For a different path, the effective stress ratio will be different. As shown in Fig. 17, there is a range of 1.5 km within which the effective stress ratio is greater than 1. Also, because the absolute values of stress components are in the sequence of $\sigma_x > \sigma_y > \sigma_z$, thus its stress pattern is the so-called "reverse faulting," although there is no fault structure there.

To better explain the range of area in which the stress pattern is "reverse faulting" within the subsalt formation, investigations on the distribution of stress components along Path 2 and Path 3 are presented in the following contexts.

As shown in Fig. 18, Path-2 is selected within the salt body. Fig. 19 shows that

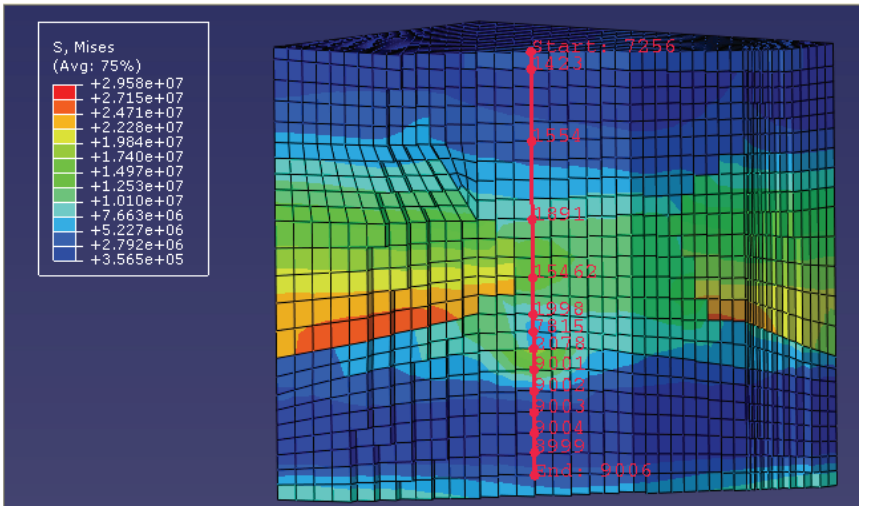

Figure 12: Illustration of Path-1 along which the stress distribution will be plotted.

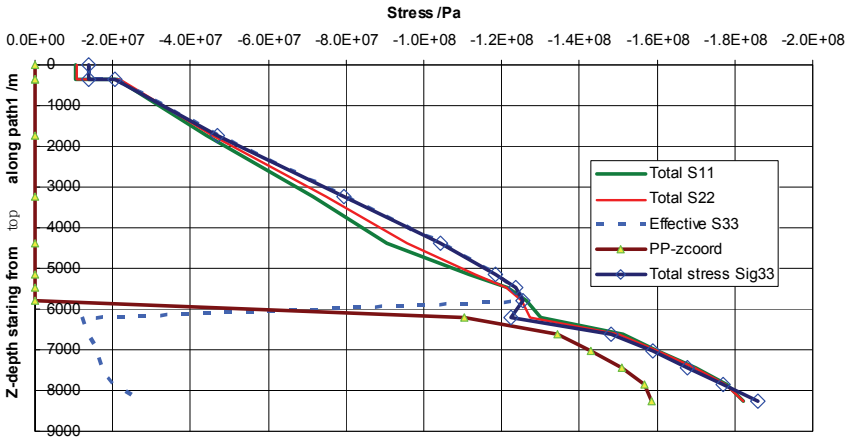

Figure 13: Variation of stress components with z-depth from the top surface.

the stress distribution along Path-2 inside the salt body is in the order of $\sigma_z > \sigma_y > \sigma_x$, which indicates the stress pattern known as "normal faulting."

As shown in Fig. 20, Path-3 is chosen within the subsalt formation and is horizontal. Fig. 21 shows the distribution of stress components along Path-3. Fig. 21 illustrates a region (marked with blue-dashed circle) whose stress components is in

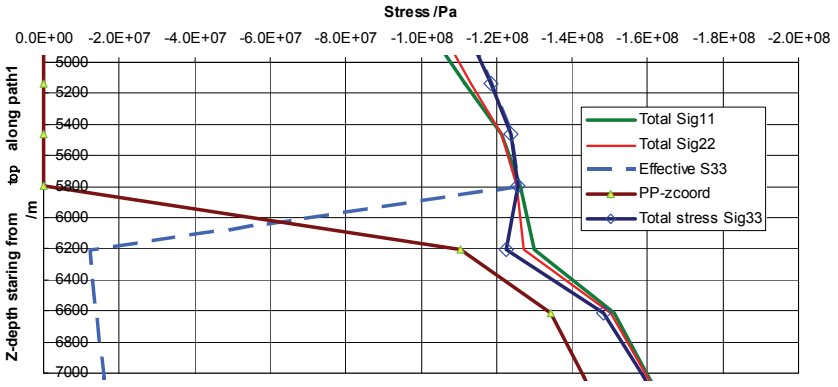

Figure 14: Zoomed-in view of stress variation with depth.

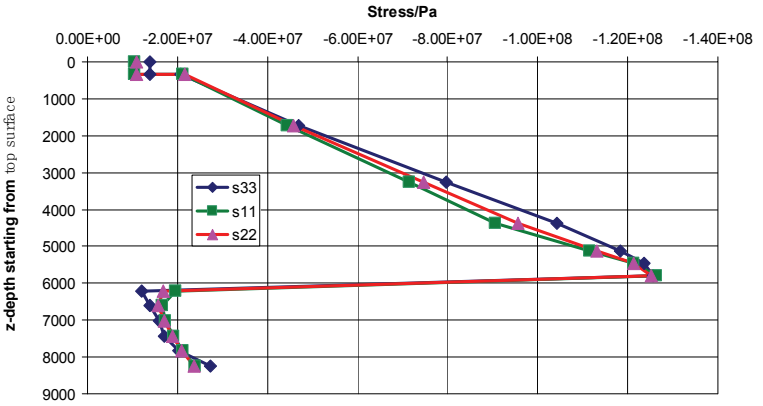

Figure 15: Distribution of effective stress ratio along Path-1.

the order of $\sigma_x > \sigma_y > \sigma_z$, which represents the stress pattern known as "reverse faulting." Other places outside the RF circle are normal fault regions, where $\sigma_z > (\sigma_y$ and $\sigma_x)$

With reference to the numerical results shown in Figs. 14, 17 and 21, it can be concluded that the stress pattern of "reverse faulting" causes the discrepancy between the results of mud-weight window obtained by using 3-D FEM and those of the 1-D method.

Because there is no faulting structure existing in the subsalt formation, it is hard to

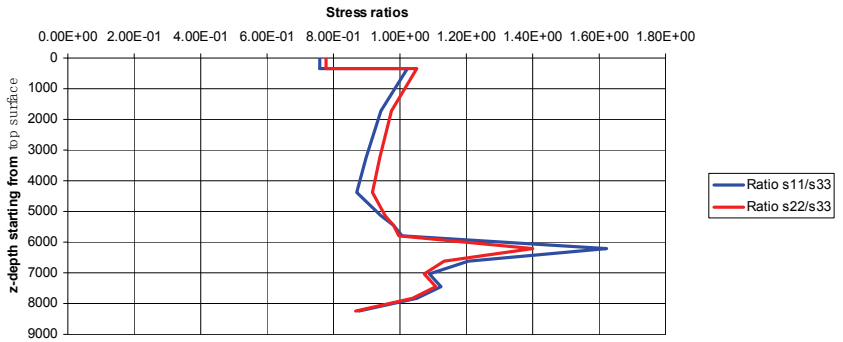

Figure 16: Distribution of effective stress ratio along Path-1.

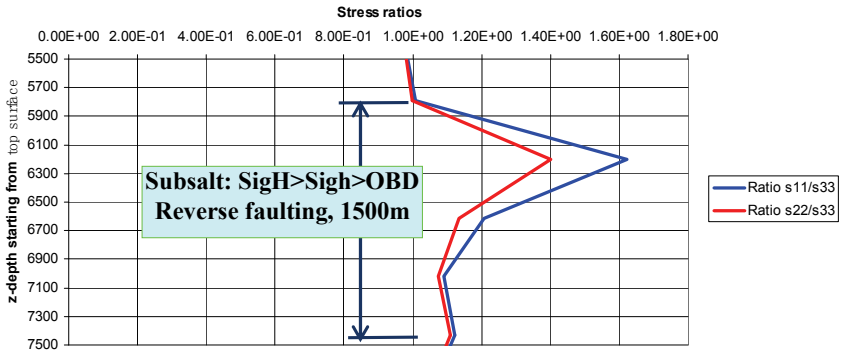

Figure 17: Distribution of effective stress ratio along Path-1: Zoomed-in view around the salt-reservoir interface.

relate its stress pattern to the form of "reverse faulting." Consequently, in the input data of the 1-D calculation for the mud-weight window, the effective-stress ratio can, thus, usually be classified as "normal faulting".

However, this kind of stress pattern can be discovered using 3-D FEM numerical calculations, although it is not used as input data there.

Fig. 22 shows an example of mud-weight logging data reported by Shen (2009). It is seen that the mud weight used in the drilling of the subsalt wellbore section (the curve in black) is higher than the overburden gradient, which indicates that the minimum horizontal stress component is higher than the vertical component and, consequently, shows an example of "reverse-faulting" stress pattern in the subsalt

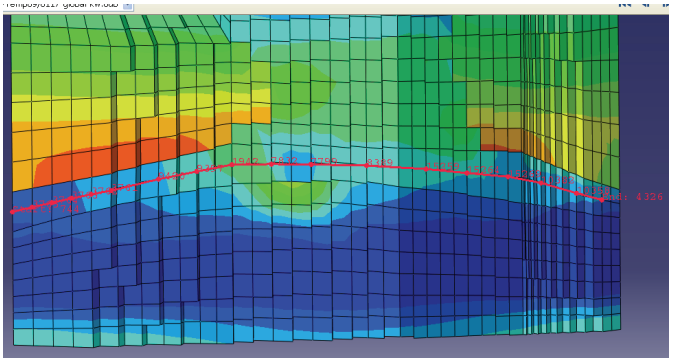

Figure 18: Illustration of Path-2.

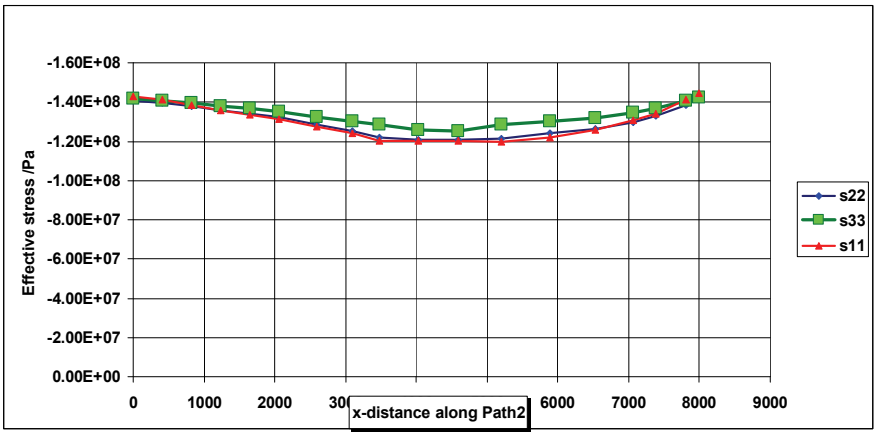

Figure 19: Distribution of effective stress components along Path-2.

formation.

5 Conclusions

Using FEM, a 3-D numerical solution of mud-weight window has been obtained for a subsalt wellbore section. Based on the numerical results presented here, the following conclusions can be obtained:

There is a region at subsalt formation where the reverse-faulting stress pattern may be formed. It is most likely to be true, particularly when there is anticline structure existing at the salt base.

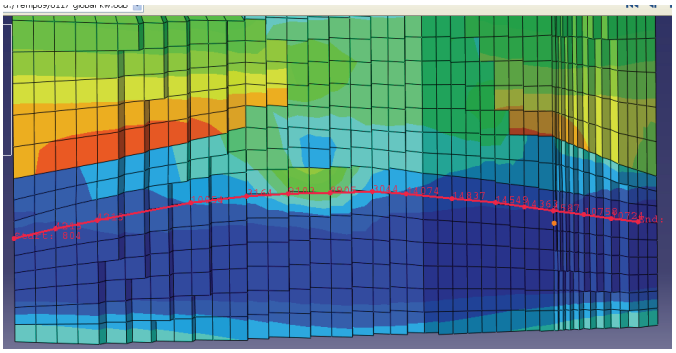

Figure 20: Illustration of Path-3.

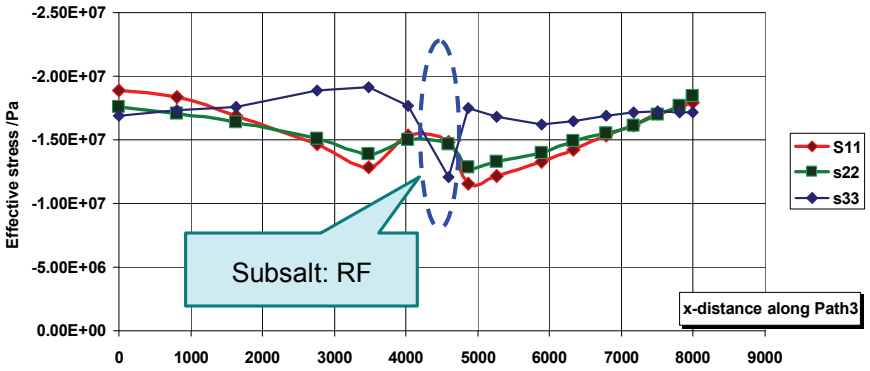

Figure 21: Distribution of stress components along Path-3.

As the wellbore trajectory goes through this region, FG and SFG at this region may appear at abnormally high values. Consequently, the mud-weight window obtained for this wellbore trajectory shown in the results is shifted/higher from the normal ones compared to the 1-D solution obtained with 1-D software.

References

Cullen, P.C., Taylor, J.M.R., Thomas, W.C., Whitehead, P., Brudy, M., and vander Zee, W. 2010. Technologies to Identify Salt- related Deep-water Drilling Hazards. OTC 29854 presented at the 2010 Offshore Technology Conference, Houston, TX, 3–6 May.

Dusseault, M.B., Maury, V., Sanfilippo, and F., Santarelli, F.J. 2004. Drilling

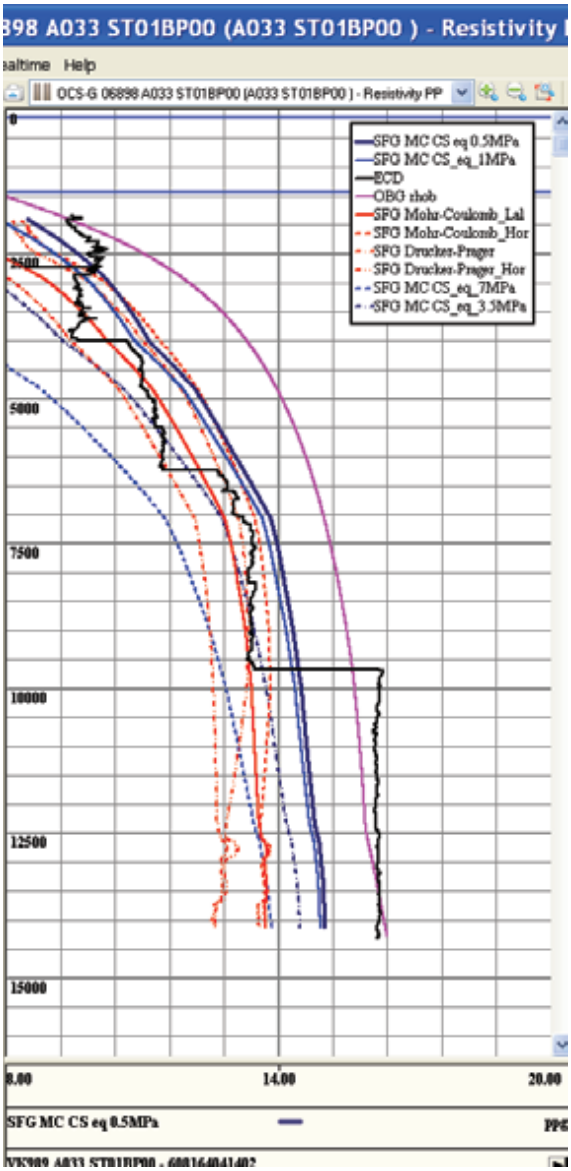

Figure 22: An example of mud-weight logging data used in practice.

through salt: constitutive behavior and drilling strategies. Paper ARMA/NARMS 04-608 Gulf Rock 2004 presented at the 6th North America Rock Mechanics Symposium, Houston, TX, 5–9 June.

Fredrich, J.T., Coblentz, D., Fossum, A.F. and Thorne, B.J. 2003. Stress Perturbation Adjacent to Salt bodies in the Deepwater Gulf of México. Paper SPE 84554 presented at the Annual Technical Conference and Exhibition, Denver, CO, 5–8 October.

Power, D., Ivan, C.D., and Brooks, S.W. 2003. The top 10 lost Circulation Concerns in Deepwater Drilling. Paper SPE 81133 presented at the SPE Latin American and Caribbean Petroleum Engineering Conference, Port of Spain, Trinidad, West Indies, 27–30 April.

Shen, X.P. 2009. DEA-161 Joint Industry Project to Develop an Improved Methodology for Wellbore Stability Prediction: Deepwater Gulf of Mexico Viosca Knoll 989 Field Area. Halliburton Consulting, Houston, Texas, USA, 18 August.

Tsai, F.C., O'Rouke, J.E., and Silva, W. 1987. Basement Rock Faulting as a Primary Mechanism for Initiating Major Salt Deformation Features. Paper presented at the 28th US Symposium on Rock Mechanics, Tucson, Arizona, 29 June–1 July.

Whitson, C.D., and McFadyen, M.K. 2001. Lesson Learned in the Planning and Drilling of Deep, Subsalt wells in the Deepwater Gulf of Mexico. Paper SPE 71363 presented at the SPE Annual Technical Conference and Exhibition, New Orleans, LA, 30 Sep–3 October.

Willson S.M. and Fedrich J.T. 2005. Geomechanics Considerations for Through- and Near-Salt Well Design. Paper SPE 95621 presented at the 2005 SPE Annual Technical Conference and Exhibition, Dallas, TX, 9–12 October.